CENTER FOR ASTROPHYSICS
HARVARD & SMITHSONIAN

Non-linear Joint Inversion of NOx and NMVOC Emissions Using Satellite Observations over East Asia

Amir H. Souri[1], Caroline R. Nowlan[1], Gonzalo González Abad[1], Lei Zhu[1,2], Donald R. Blake[3], Alan Fried[4], Andrew J. Weinheimer[5], Armin Wisthaler[6], Jung-Hun Woo[7], Qiang Zhang[8], Christopher E. Chan Miller[1], Xiong Liu[1], and Kelly Chance[1]

[1]Harvard-Smithsonian [2]SusTech [3]UCI [4]UC-Boulder [5]NCAR [6]Oslo [7]Konkuk [8]Tsinghua

Oct 2020 - CMAS Meeting - Virtual

Sponsored by:

NASA

Aura Science Team, MEASURES, and Science of Terra, Aqua, and Suomi NPP

NATIONAL OCEANIC AND ATMOSPHERIC ADMINISTRATION
NOAA
U.S. DEPARTMENT OF COMMERCE

NOAA AC4 Program

Background

- The absence of updated emissions has been a major impediment to sufficiently simulate different aspects of atmospheric chemistry.
- Bottom-up emissions inventories:
  - Fuel combustion (mobile, power plants and etc.)
  - Biomass burning (satellite data and fuel information)
  - Lightning (convective parametrization)
  - Biogenic emissions (microbial processes in soil, plants functional maps, emission factors, resistance calculations)
- The bottom-up emissions are subject to errors and being obsolete.

Objective

- Any relevant data can be used to constraint the bottom-up emissions. (as relevant (linear) as possible!)
- Having well-characterized satellite observations may improve the bottom-up estimates for those areas undergoing **larger** errors (or bigger changes) in emissions compared to the uncertainty associated with satellites-based measurements (projected onto the emission space).
- **We will attempt to constrain both NO_x and VOC emissions using OMI and OMPS:**
  - ✓This will enable us to constrain the ozone production rates.
  - ✓The chemical feedback existing between NO_x-HCHO and VOC-NO_2 is considered.
  - ✓We will be able to quantify the impact of the recent changes in anthropogenic emissions in East Asia on ozone pollution.

Data (NO_2)

- We use NASA OMI tropospheric NO_2 (version 3.1) level 2 data whose retrieval is based on the violet/blue (402-465 nm) due to its strong absorption in this wavelength range.
- The sensor has a nadir spatial resolution of 13×24 km^2 which can extend to 40×160 km^2 at the edge of scanlines.
- We remove bad pixels based on cloud fraction < 20%, solar zenith angle < 65^o, without the row anomaly, vertical column density (VCD) quality flag = 0, and Terrain Reflectivity < 30%.
- We recalculate AMFs using shape factors derived from the chemical transport model used in this study. We oversample the OMI granules using the Cressman interpolator with a 0.25^o radius of influence.

Data (HCHO)

- OMPS-NM onboard the Suomi National Polar-orbiting Partnership (Suomi NPP) is a UV-backscattered radiation spectrometer launched in October 2011
- The sensor has a 340×740 pixel CCD array measuring the UV spectra at a spatial resolution of 50×50 km^2 at nadir.
- OMPS HCHO algorithm follows the SAO algorithm [Gonzalez et al., 2016] in the spectral range 327.7-356.5 nm.
- We use earthshine radiances over a relatively clear area in the remote Pacific Ocean within -30^o to $+30^o$ latitudes.
    - An upgrade to this reference correction is the use of daily HCHO profiles over the mean climatological ones from simulations done by the GEOS-Chem chemical transport model.
- We remove unqualified pixels based on cloud fraction < 40%, solar zenith angle < 65^o, a main quality flag provided in the data.
- We recalculate AMF using a regional model, and use the Cressman spatial interpolator with a 1^o radius of influence for oversampling.

OMI had depreciated a lot.

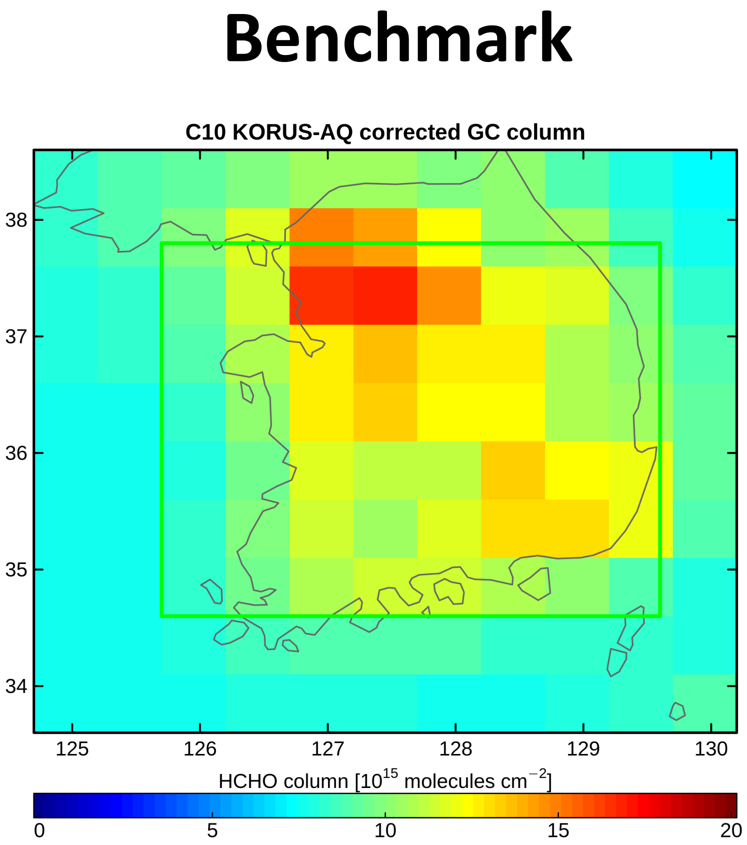

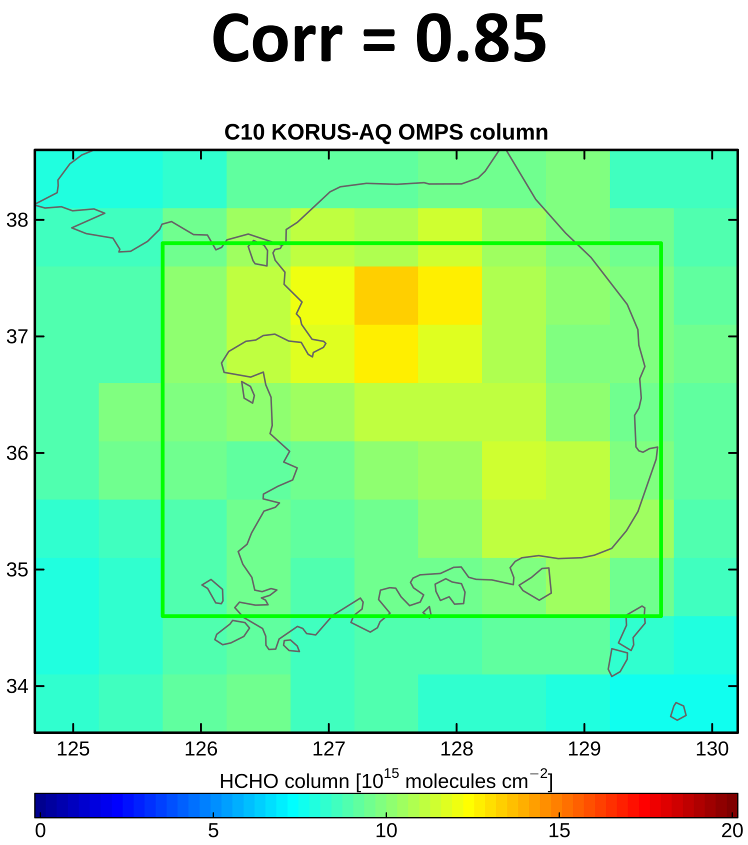

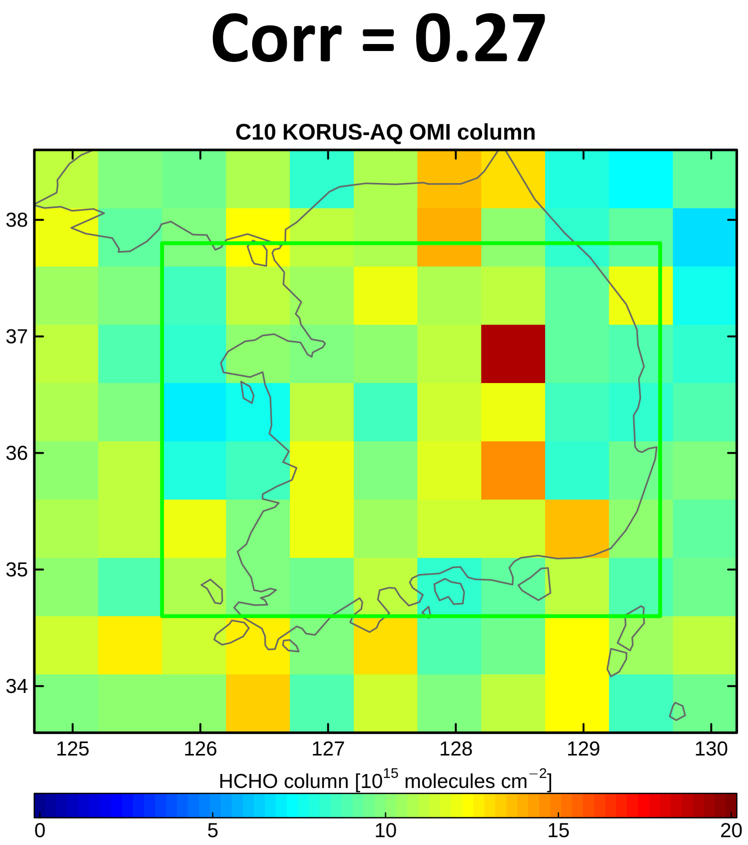

Model (WRF-CMAQ)

- We simulate the atmospheric composition in East Asia using **the CMAQ model** [Byun and Schere, 2006] at 27 km spatial resolution with 328×323 grid size.
- May-June 2016.
- We choose the **CB05** gas-phase mechanism, which includes chlorine chemistry and the six-generation aerosol mechanism (**AERO6**) which considers sea salt and aqueous/cloud chemistry.
- We process anthropogenic emissions for the CMAQ domain from the **MIX emissions inventory 2010** [Li et al., 2015].
- The **FINN v1.6** emissions [Wiedinmyer et al., 2011] are extended to include biomass burning emissions.
- We use a standalone **MEGAN (v2.1)** [Guenther et al., 2006] model to include biogenic emissions.
- The diurnally lateral chemical conditions are generated by GEOS-Chem v10 [Bey et al., 2001] with the full chemistry mechanism (NO_x-O_x-HC-Aer-Br) spun up for a year.

Model (WRF-CMAQ)

- In order to simulate the mesoscale meteorology, we use the Weather Research and Forecasting model (WRF) v3.9.1 [Skamarock et al., 2008].
- The lateral boundary conditions and the grid nudging inputs come from the global Final (FNL) 0.25^{o} resolution model.
- Physical options include: **KF** sub-grid cumulus parametrization **WSM-6** for microphysics, **ACM2** scheme for the planetary layer fluxes, **Noah** Land-Surface Model for the surface physics, and Rapid Radiative Transfer Model (**RRTM**) for short- and long-wave radiation.

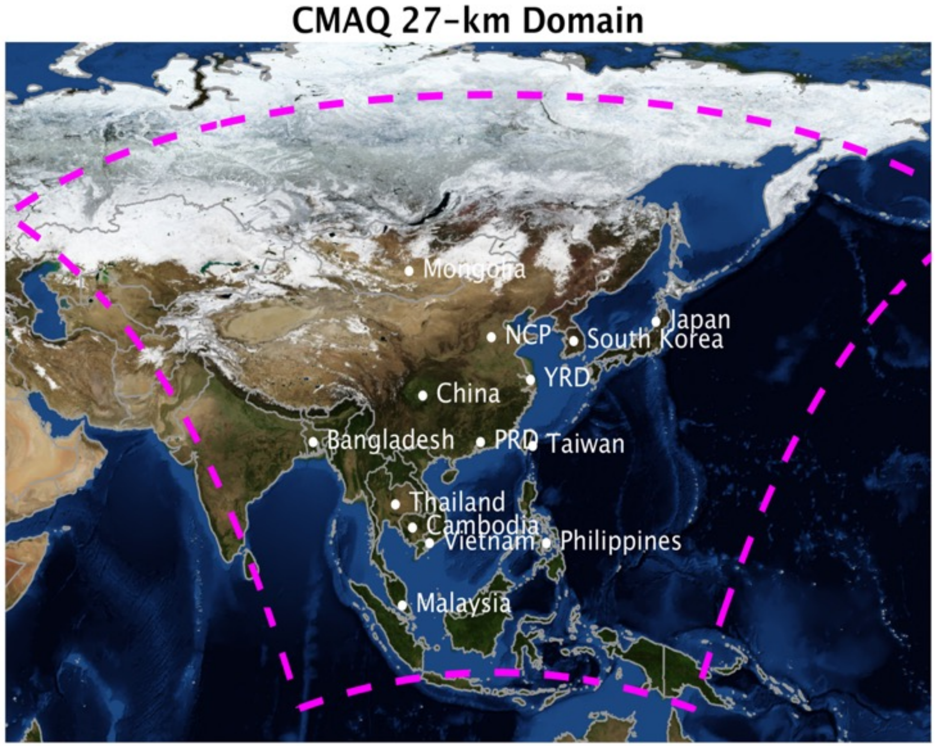

Inverse Modeling (Analytical)

- The inversion seeks to solve the following cost function under the assumptions that i) both observation and emission error covariances follow Gaussian probability density functions with a zero bias, ii) the observation and emission error covariances are independent and iii) the relationship between observations and emissions is not grossly non-linear:
- $J(\mathbf{x}) = \frac{1}{2}(\mathbf{y} - F(\mathbf{x}))^T \mathbf{S}_o^{-1}(\mathbf{y} - F(\mathbf{x})) + \frac{1}{2}(\mathbf{x} - \mathbf{x}_a)^T \mathbf{S}_e^{-1}(\mathbf{x} - \mathbf{x}_a)$
- where ***x*** is the inversion estimate (the a posteriori) given two sources of data: the a priori ($\boldsymbol{x}_a$) and observation ($\boldsymbol{y}$). $\mathbf{S}_o$ and $\mathbf{S}_e$ are the error covariance matrices of observation (instrument) and emission. *F(**x**)* is the the forward model.

Inverse Modeling (Optimization)

- **Gauss-Newton method:**
  - $\mathbf{x}_{\boldsymbol{i}+\mathbf{1}} = \mathbf{x}_a + \mathbf{G}[\mathbf{y} - F(\mathbf{x}_{\boldsymbol{i}}) + K_i(\mathbf{x}_{\boldsymbol{i}} - \mathbf{x}_a)]$
  - $\mathbf{G} = \mathbf{S}_e\ K_i^T\left(K_i\mathbf{S}_e\ K_i^T + \mathbf{S}_o\ \right)^{-1}$
  - $\hat{\mathbf{S}}_e\ = (\mathbf{I} - \mathbf{G}\widehat{K}^T)\mathbf{S}_e$
  - $\mathbf{A} = \mathbf{I} - \hat{\mathbf{S}}_e\mathbf{S}_e^{-1}$

- *K* is calculated by CMAQ-DDM (which calculates the first derivative concentrations to emissions)
- K_i (= $K(\mathbf{x}_{\boldsymbol{i}})$)
- Here we iterate the optimizer three times.
- A explains the amount of information gained from observations.

Inverse Modeling (Chemical Feedback)

CMAQ-DDM

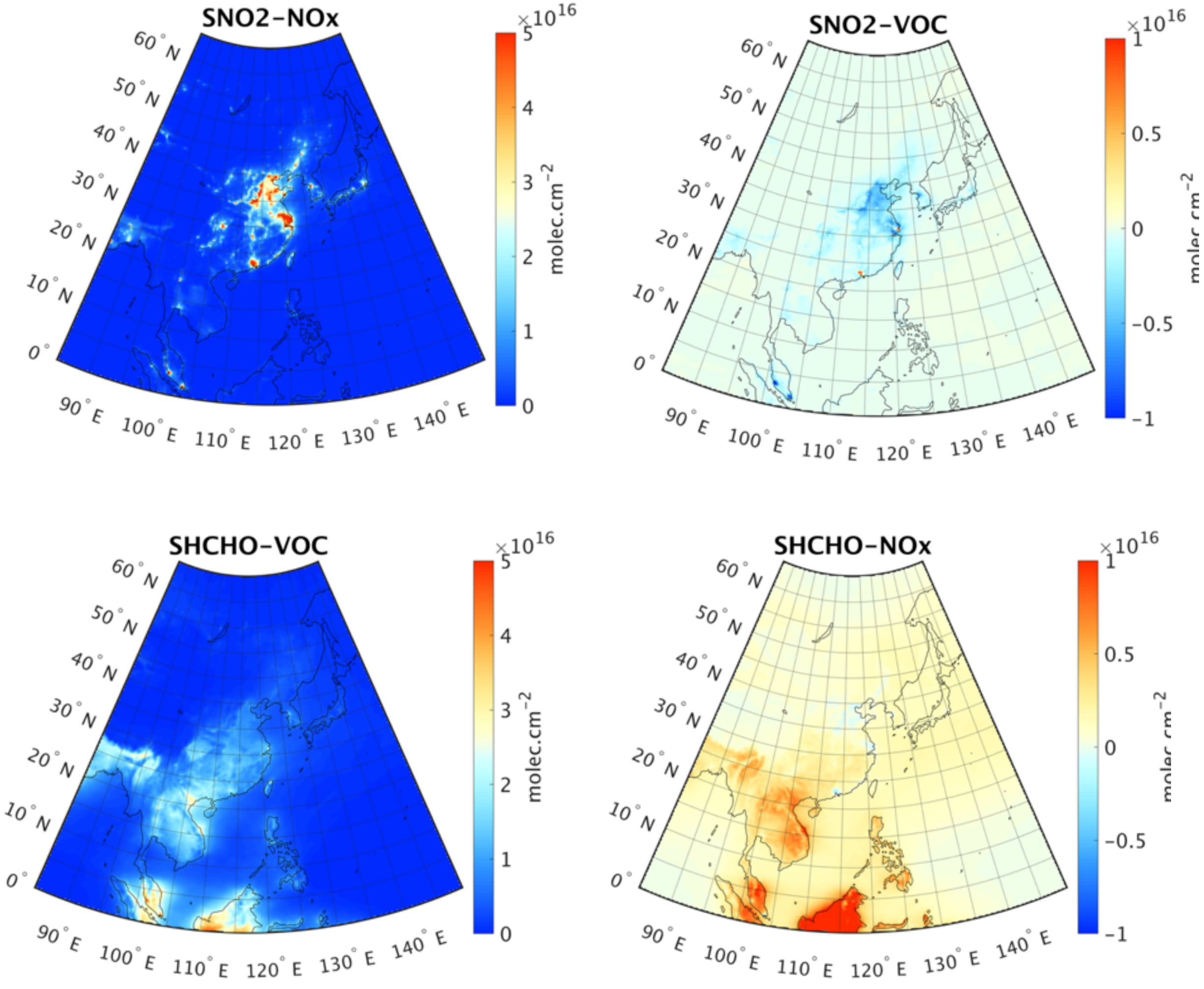

F0AM Box Model

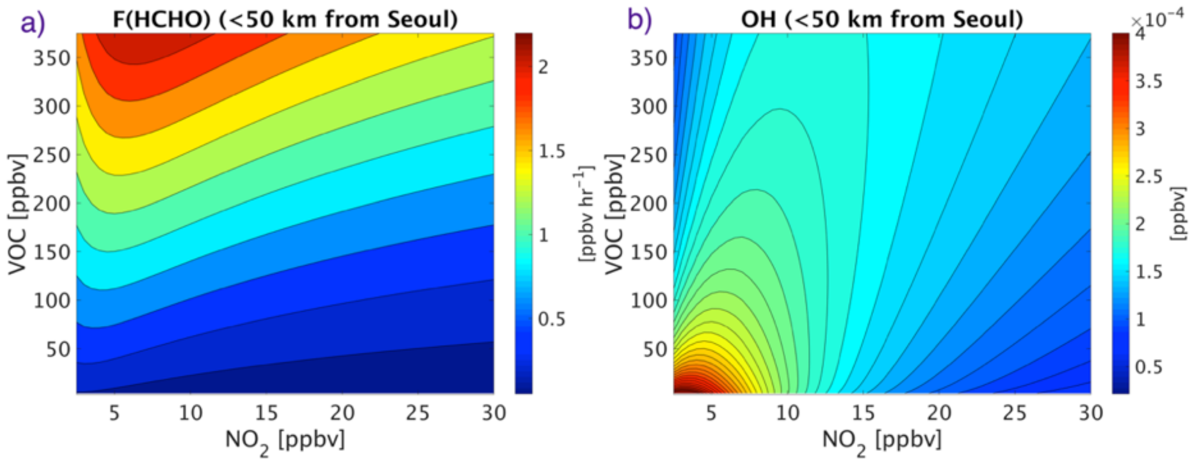

Souri et al., 2020, AE

Inverse Modeling (Observation errors)

- **Errors in the retrieval**
  - **Random errors**
    - They never cancel each other.
    - Can be significantly lowered down by oversampling (reason why we also include partially cloudy pixels).
  - **Systematic errors**
    - They can cancel each other.
    - Should be directly added/removed to the observations.
- In practice, there is no "the truth" to determine the exact systematic errors, so there is <u>an error in the systematic error estimation</u> that should be added to S_o
- We followed Zhu et al. [2020]'s intercomparison platform using KORUS-AQ data over the Korean Peninsula to calculate the bias (-20%) and the errors associated with.
- Regarding NO_2, we followed Choi et al. [2019]. We uniformly scaled up NO_2 by by 33.9% (see table A3 in the paper).
- Random errors are derived from the column uncertainty variables, AMFs (20%).

Inverse Modeling (Emission errors)

- A general rule thumb says anthropogenic emissions (50%) are less uncertain than biogenic ones (100-300%).
- To increase the degree of freedom for the optimization, we combine all sector emissions including anthropogenic, biomass burning and biogenic emissions for NO_x and VOCs. Therefore, we use the following formula to estimate the covariance of the a priori:
- $\sigma^2_{Total} = f^2_{Anthro} \times \sigma^2_{Anthro} + f^2_{BB} \times \sigma^2_{BB} + f^2_{Bio} \times \sigma^2_{Bio}$

	Anthropogenic	Biogenic	Biomass Burning
NO_x	50%	200%	100%
VOC	150%	200%	300%

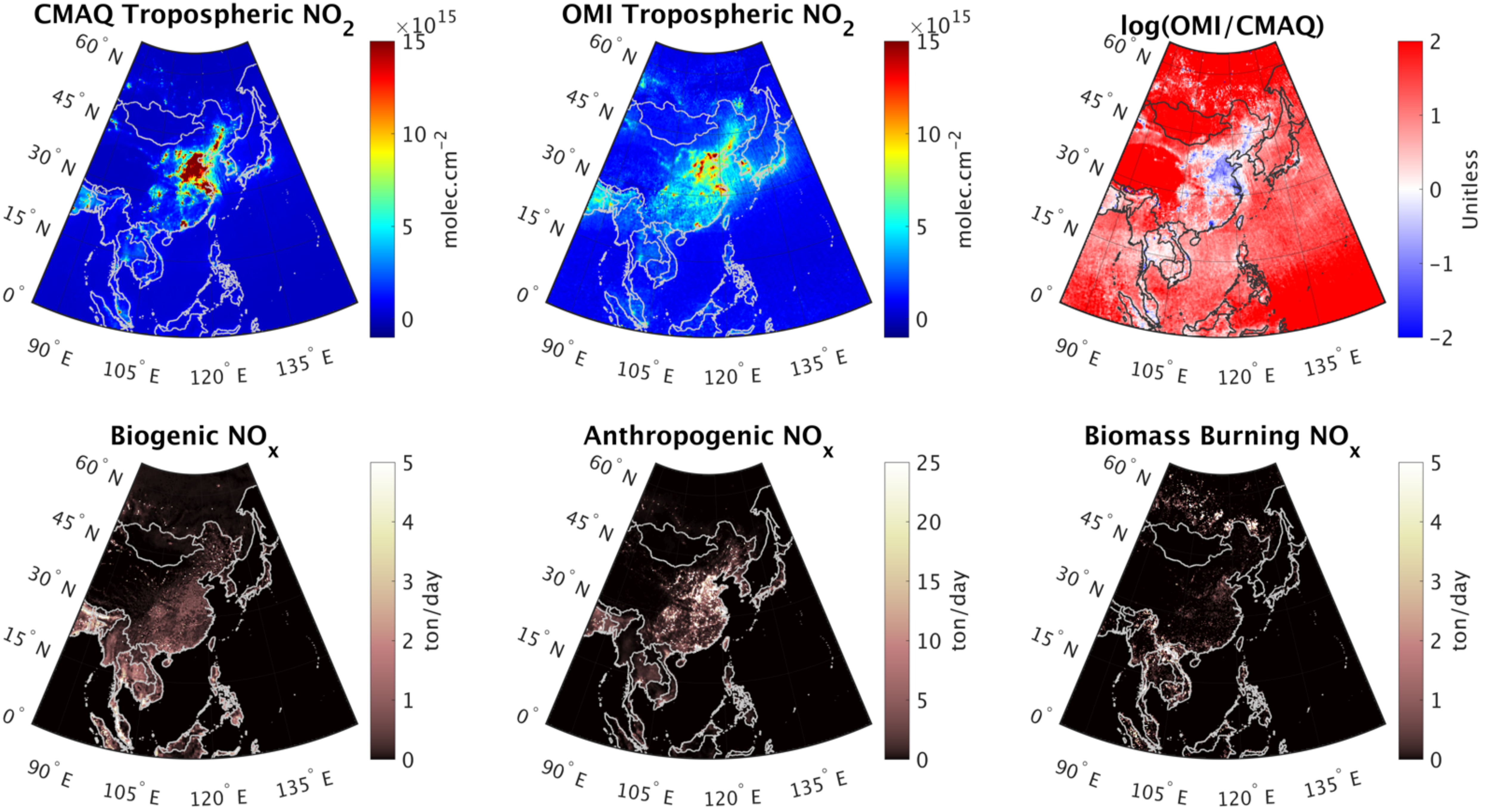
CMAQ Tropospheric NO2
OMI Tropospheric NO2
log(OMI/CMAQ)
×10^15
molec.cm^-2
Unitless
Biogenic NOx
Anthropogenic NOx
Biomass Burning NOx
ton/day
60° N
45° N
30° N
15° N
0°
90° E
105° E
120° E
135° E

Consistent with OMI Tropospheric NO_2 trends

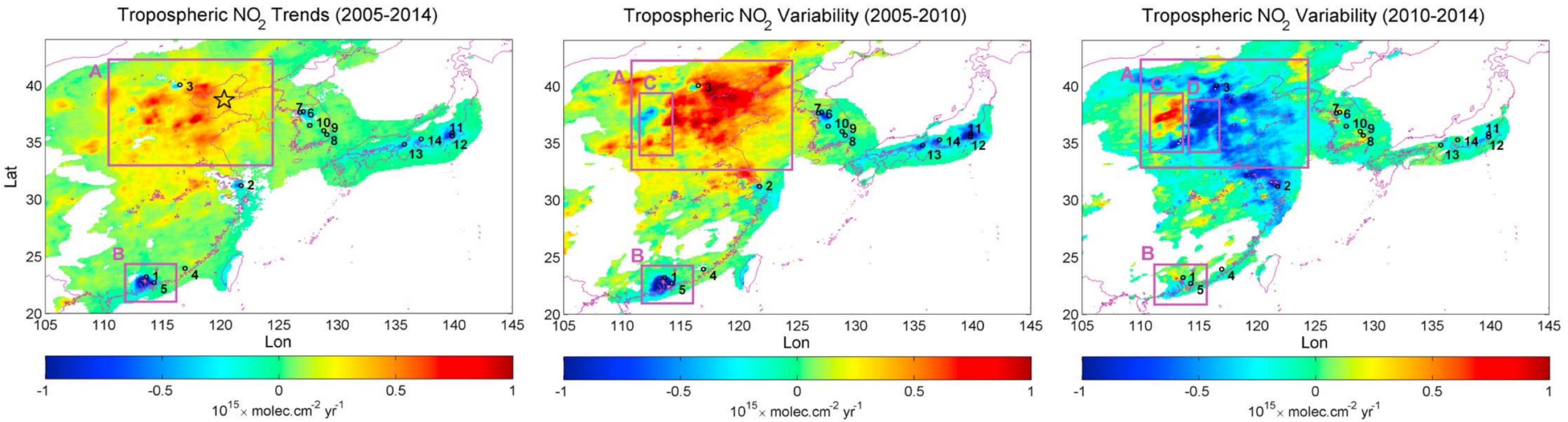

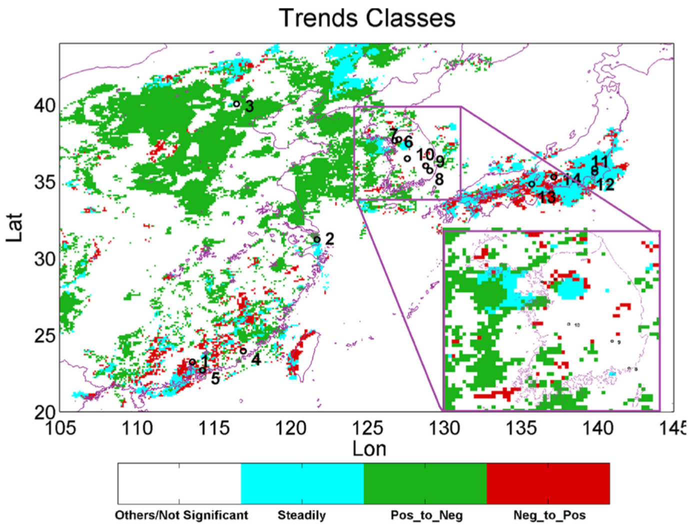

Souri et al., 2017, JGR

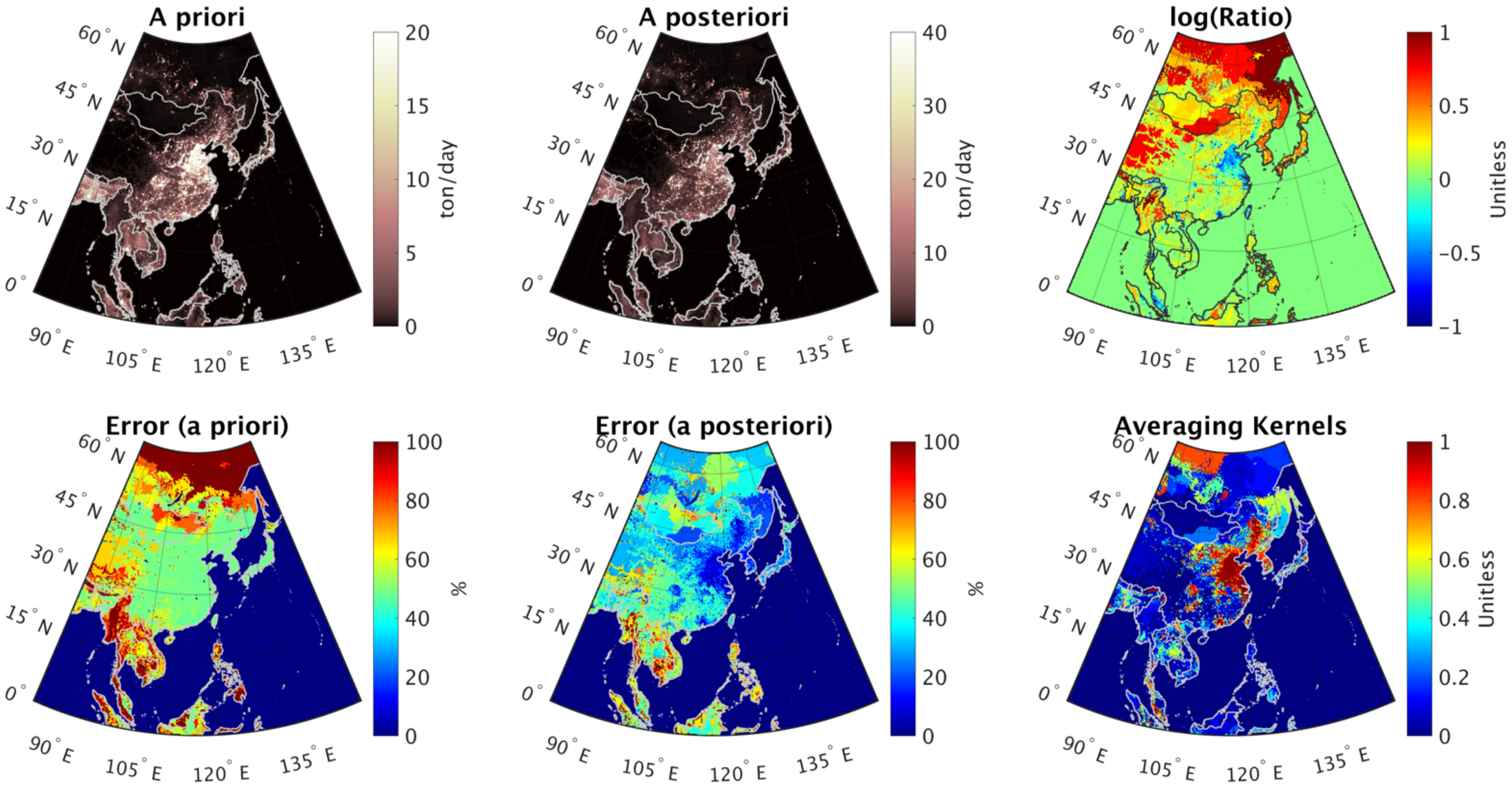

A priori
A posteriori
log(Ratio)
Error (a priori)
Error (a posteriori)
Averaging Kernels
ton/day
%
Unitless
60° N
45° N
30° N
15° N
0°
90° E
105° E
120° E
135° E

Numbers for NO_x

Table 1. NO_x emissions before and after carrying out the inversion for different countries in May-June 2016.

Countries	The a priori (Gg/day)	The a posteriori (Gg/day)	Changes in magnitudes	Changes in errors
China	87.94±44.09[1]	68.00±15.94[2]	-23%	-63%
North China Plain	27.96±13.49	19.05±2.50	-32%	-81%
Pearl River Delta	4.23±1.78	2.70±0.32	-36%	-84%
Yangtze River Delta	9.84±4.68	5.77±0.51	-41%	-89%
Thailand	4.38±3.24	4.20±2.28	-4%	-29%
Japan	3.53±1.71	3.96±1.04	+12%	-39%
Malaysia	2.89±2.77	2.25±1.34	-22%	-49%
Vietnam	2.87±2.04	2.79±1.57	-3%	-23%
South Korea	2.71±1.34	2.95±0.58	+9%	-56%
Bangladesh	1.72±1.06	2.10±0.87	+22%	-18%
Philippines	1.30±1.10	1.54±0.98	+18%	-11%
Taiwan	1.26±0.57	0.97±0.33	-23%	-42%
Cambodia	0.54±0.50	0.57±0.45	+5%	-11%
Mongolia	0.19±0.13	0.28±0.12	+44%	-8%

Validation

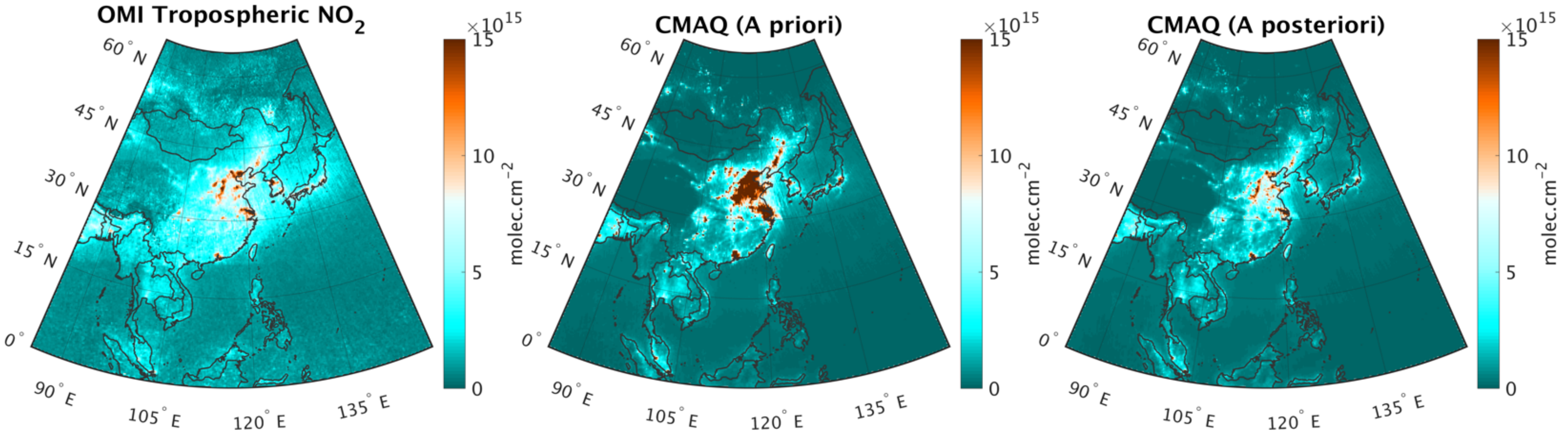

- We observe an underestimation of NO_2 at the near surface levels (<900 hPa) by 19% (DC8 = 4.50 ppbv, CMAQ = 3.67 ppbv). The updated emissions increase the near surface levels over the Korean Peninsula, which in turn, reduce the bias to 11% (CMAQ = 4.02 ppbv).

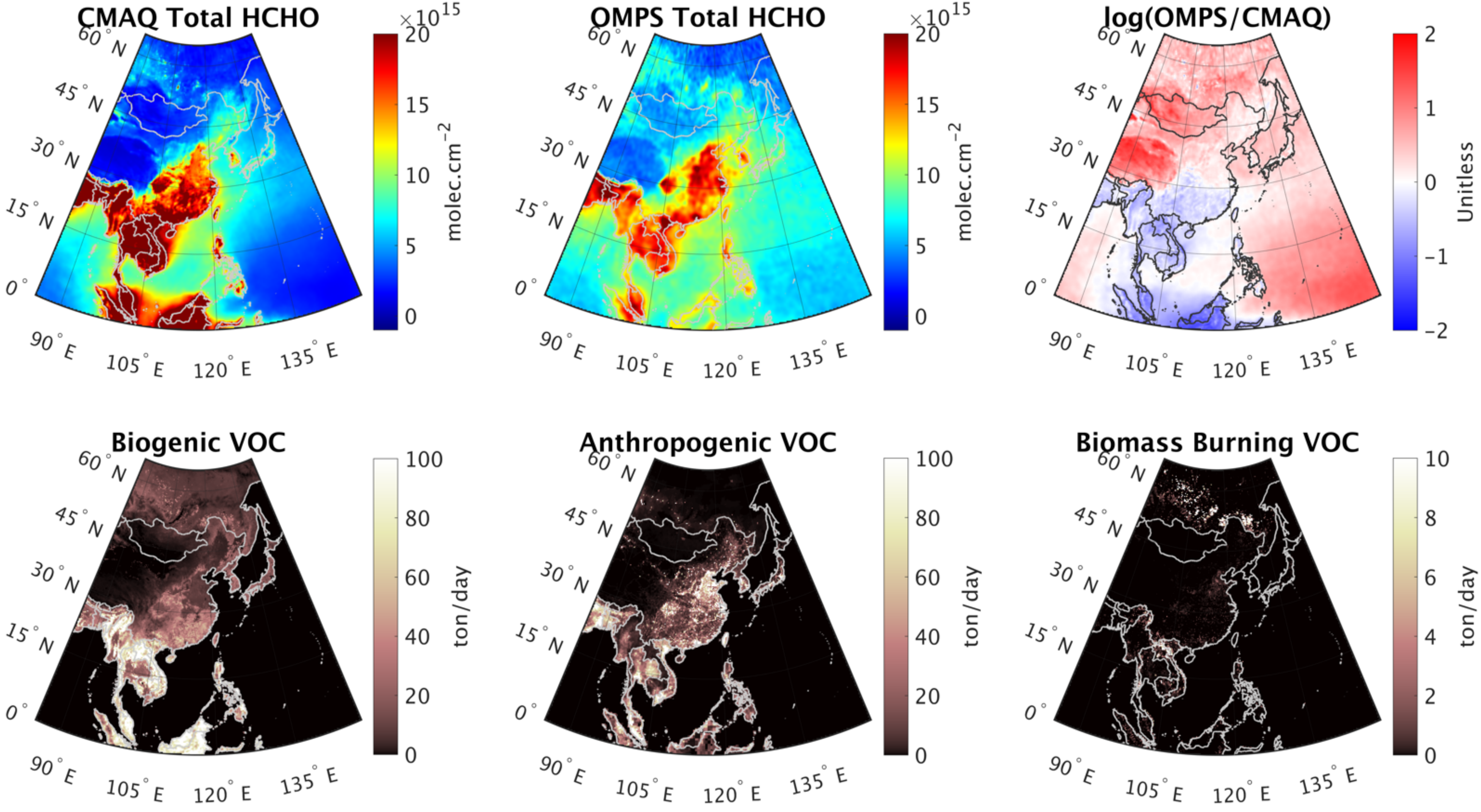

CMAQ Total HCHO
OMPS Total HCHO
log(OMPS/CMAQ)
Biogenic VOC
Anthropogenic VOC
Biomass Burning VOC
$\times 10^{15}$
molec.cm^{-2}
Unitless
ton/day
0
5
10
15
20
−2
−1
1
2
40
60
80
100
4
6
8
10
60° N
45° N
30° N
15° N
0°
90° E
105° E
120° E
135° E

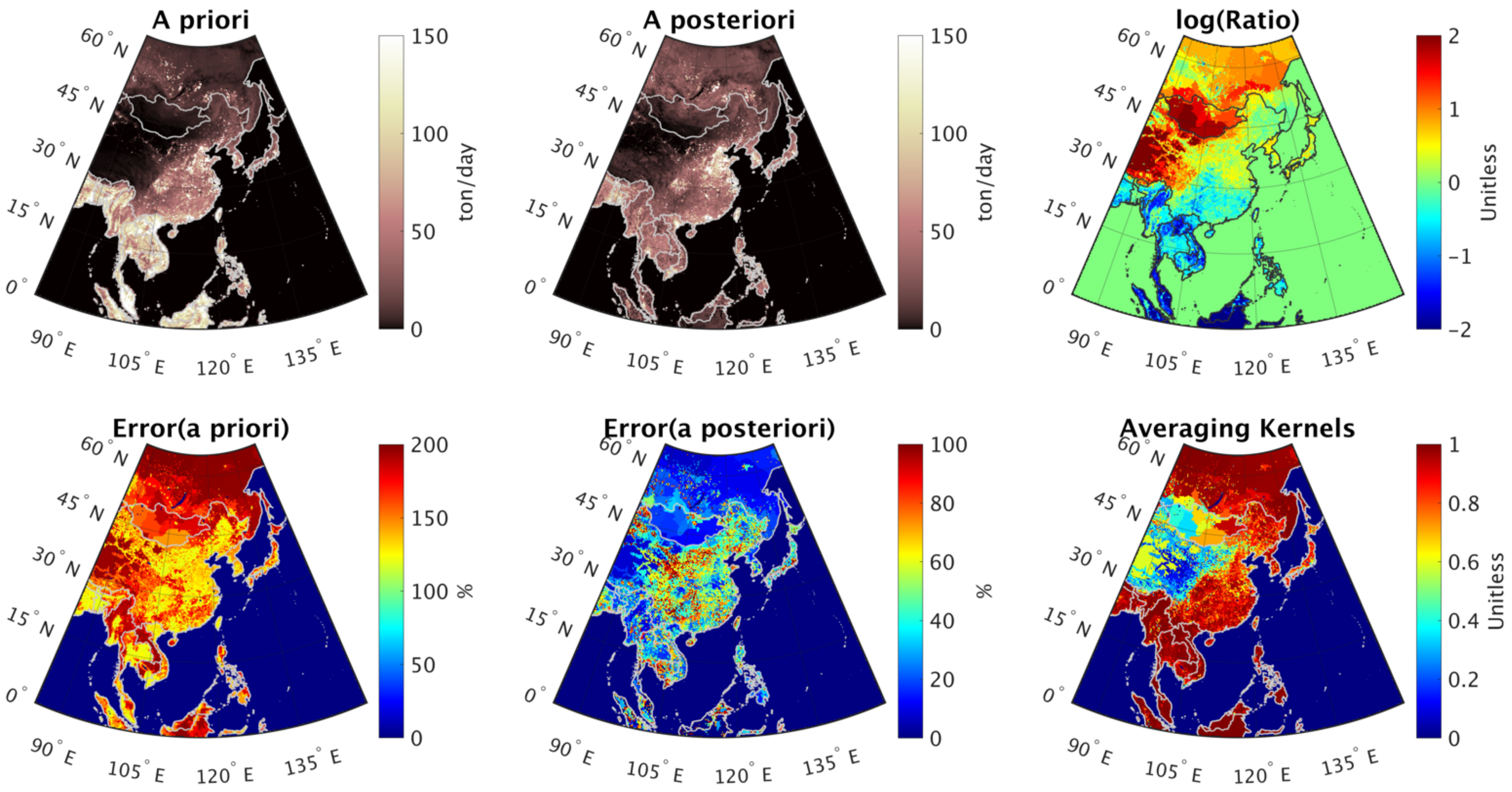

A priori
A posteriori
log(Ratio)
Error(a priori)
Error(a posteriori)
Averaging Kernels
ton/day
%
Unitless
60° N
45° N
30° N
15° N
0°
90° E
105° E
120° E
135° E
150
100
50
0
2
1
−1
−2
200
80
60
40
20
0.8
0.6
0.4
0.2

Validation

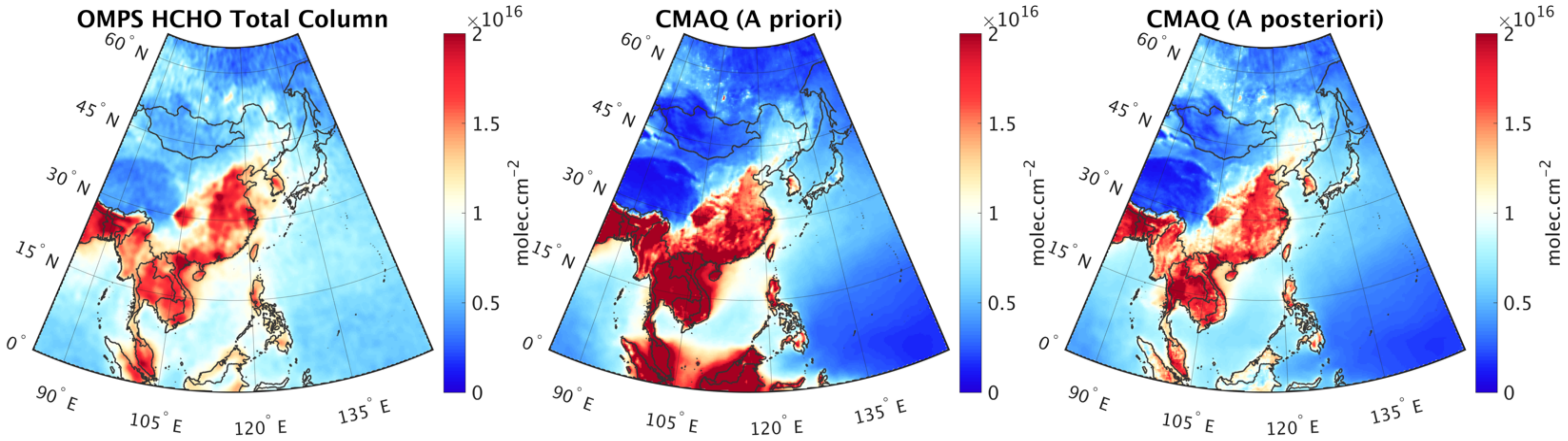

- The comparison of the simulated values with the DC-8 measurements showed a noticeable mitigation in the discrepancy between two datasets at lower boundaries (<900 hPa) in terms of isoprene, ethane, ethene, and acetaldehyde.
- We tend to underestimate HCHO concentrations (by 15%) in the lower atmosphere (<900 hPa) after using the a posteriori over the Korean Peninsula.

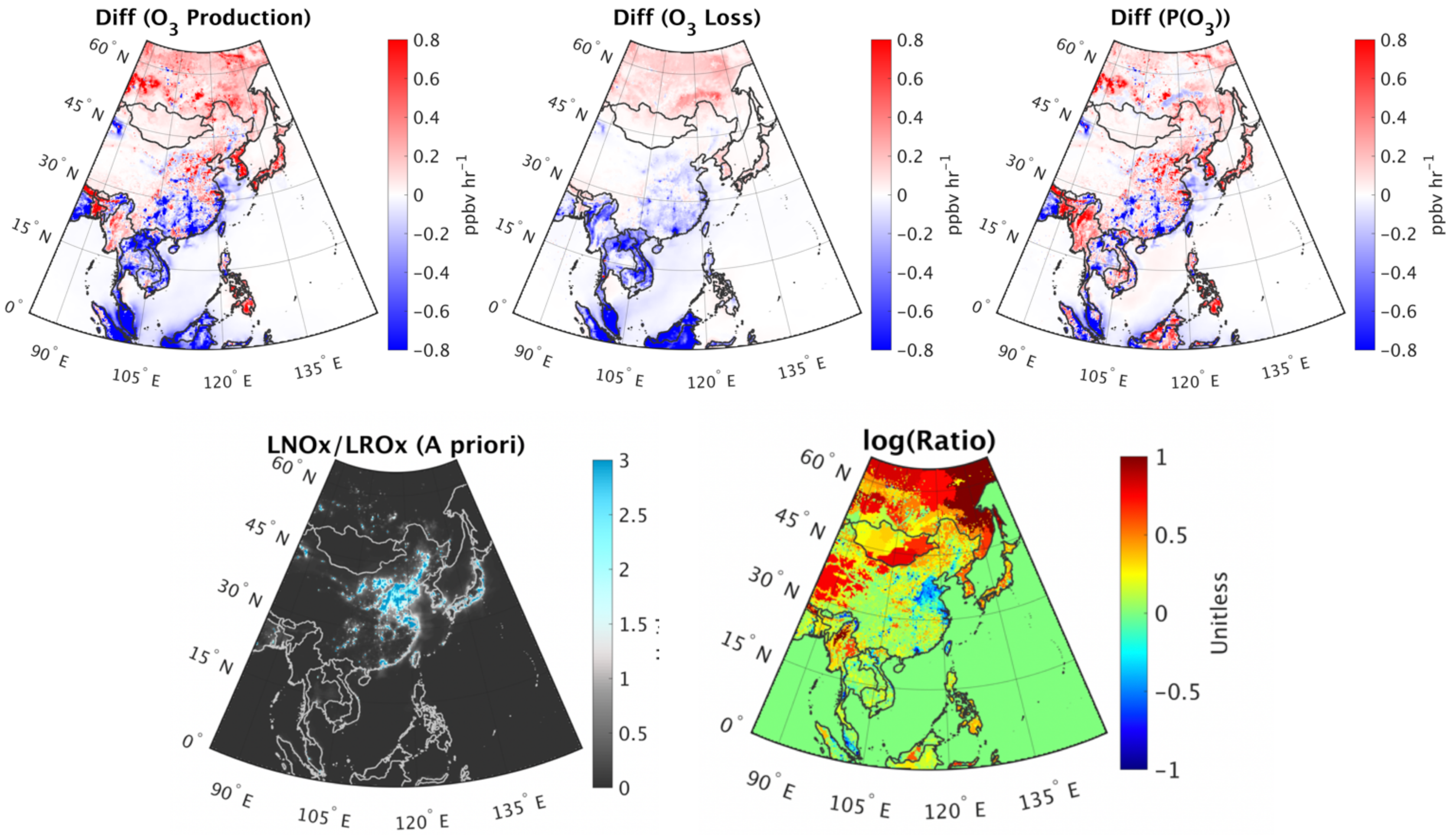

Diff (O3 Production)
Diff (O3 Loss)
Diff (P(O3))
ppbv hr−1
0.8
0.6
0.4
0.2
0
−0.2
−0.4
−0.6
−0.8
60° N
45° N
30° N
15° N
0°
90° E
105° E
120° E
135° E
LNOx/LROx (A priori)
3
2.5
2
1.5
1
0.5
0
log(Ratio)
1
0.5
0
−0.5
−1
Unitless

Ozone pollution has gotten worse in North China

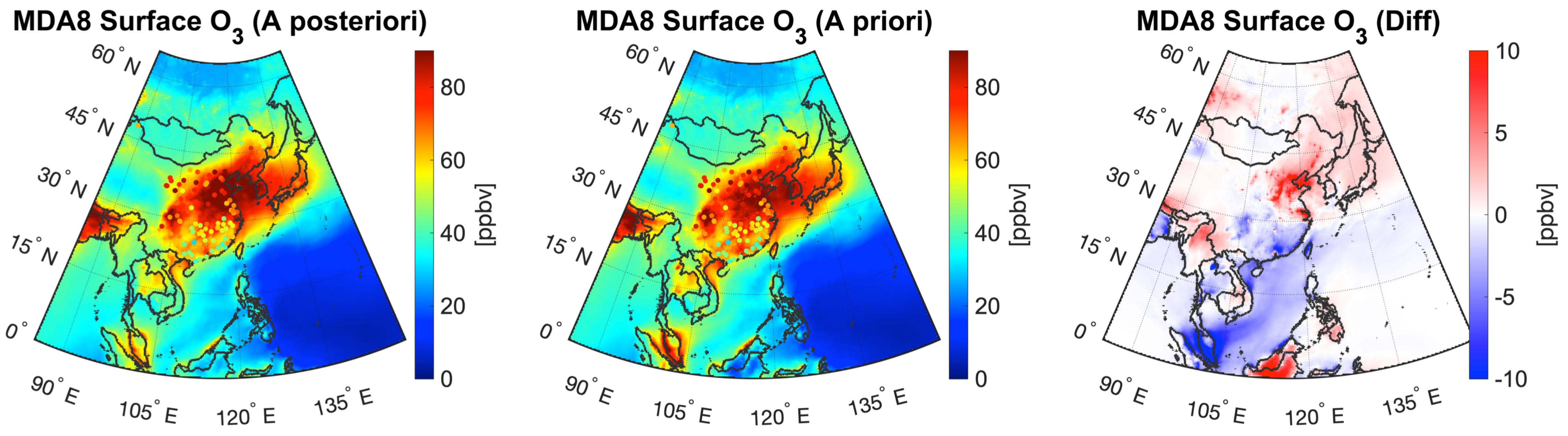

- Enhancements of maximum daily 8-hour average (MDA8) surface ozone over China (0.62 ppbv), NCP (4.56 ppbv), and YRD (5.25 ppbv) suggesting that emissions standards should be extended to regulate VOCs.
- Taiwan, Malaysia, and PRD stand out as the regions undergoing lower MDA8 ozone levels resulting from the NO_x reductions occurring predominantly in NO_x-sensitive regimes.

Conclusions

- For the first time, we performed joint non-linear analytical inversion of NO_x and VOC using satellite observations.
- OMI/OMPS bolster the capability of the CTM in terms of the simulation HCHO and NO_2 columns by providing credible top-down emissions (AKs>0.8) over polluted areas and dense vegetation.
- Low AKs in terms of NO_x in rural areas; it is desirable, but very challenging to gain information from OMI over pristine regions.

Conclusions

- Reductions of NO_x (from 2010 to 2016) in China (-23%), Taiwan (-23%), and Malaysia (-22%). Increases in NO_x in Japan (+12%) and South Korea (+9%)
- An increase in (mainly anthropogenic) VOCs in NCP by 25% since 2010.
- In NCP and YRD, a substantial reduction in afternoon NO_2+OH reaction rate (a major loss of O_3), and an increase in afternoon NO+HO_2 and RO_2+NO (a major production pathway for O_3) are observed.
  - This leads to enhancements of the simulated maximum daily 8-hr average (MDA8) surface ozone concentrations by ~5 ppbv.
- Being predominantly in NO_x-sensitive regimes favors regions including Taiwan, Malaysia and PRD to benefit from reductions in NO_x, resulting in noticeable decreases in simulated MDA8 surface ozone levels.

- Thanks for NASA Aura Science Team, NASA MEaSUREs, NOAA AC3, and NASA Science of Terra, Aqua and Suomi NPP Funds.

- For more detail: **doi.org/10.5194/acp-20-9837-2020**

Thanks for your attention!

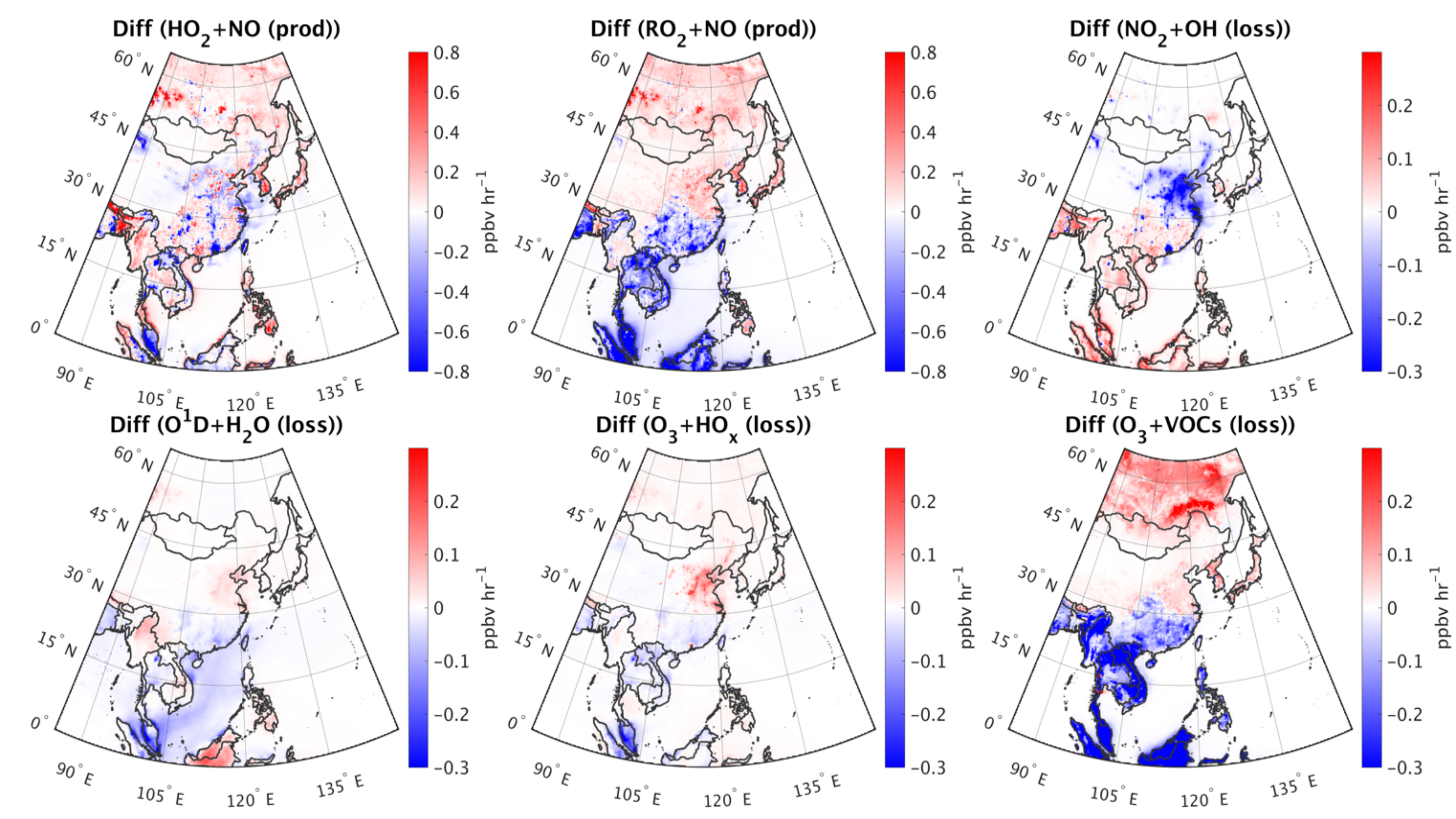

Diff (HO2+NO (prod))
Diff (RO2+NO (prod))
Diff (NO2+OH (loss))
Diff (O1D+H2O (loss))
Diff (O3+HOx (loss))
Diff (O3+VOCs (loss))
60° N
45° N
30° N
15° N
0°
90° E
105° E
120° E
135° E
ppbv hr−1
0.8
0.6
0.4
0.2
0
−0.2
−0.4
−0.6
−0.8
0.2
0.1
−0.1
−0.2
−0.3

NO2 and HCHO profiles

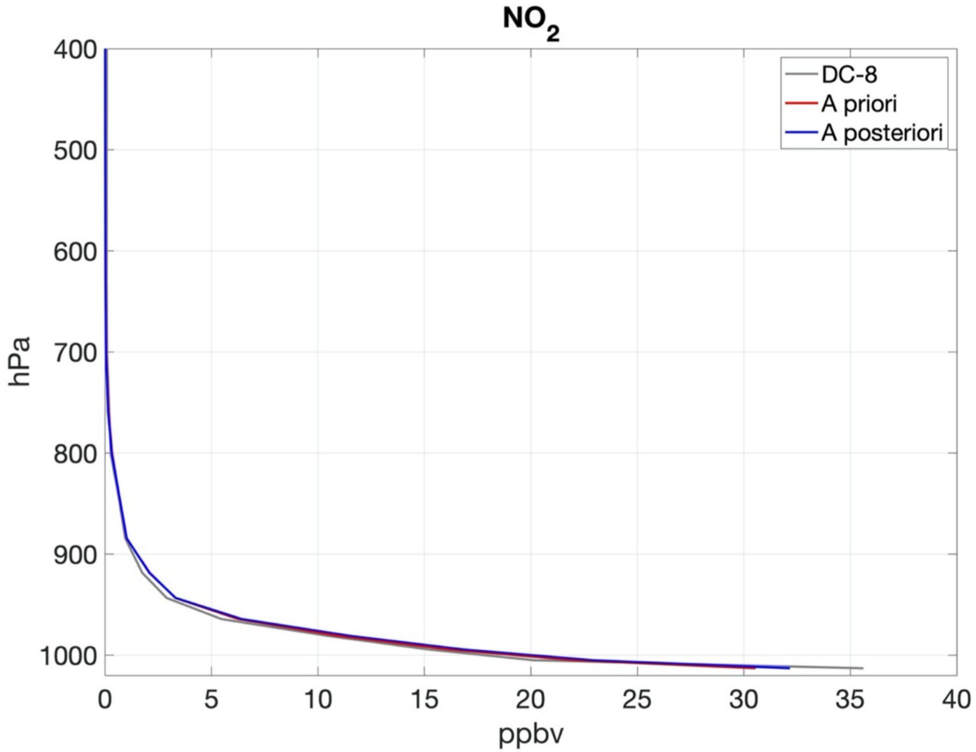

Figure S4. Comparison of the simulated model using the prior/posterior emissions and DC-8 measurements in terms of NO_2 mixing ratios. We included all 10-secs observations available from DC-8 four-channel NCAR's chemiluminescence in May-June 2016. The profiles are the mean average.

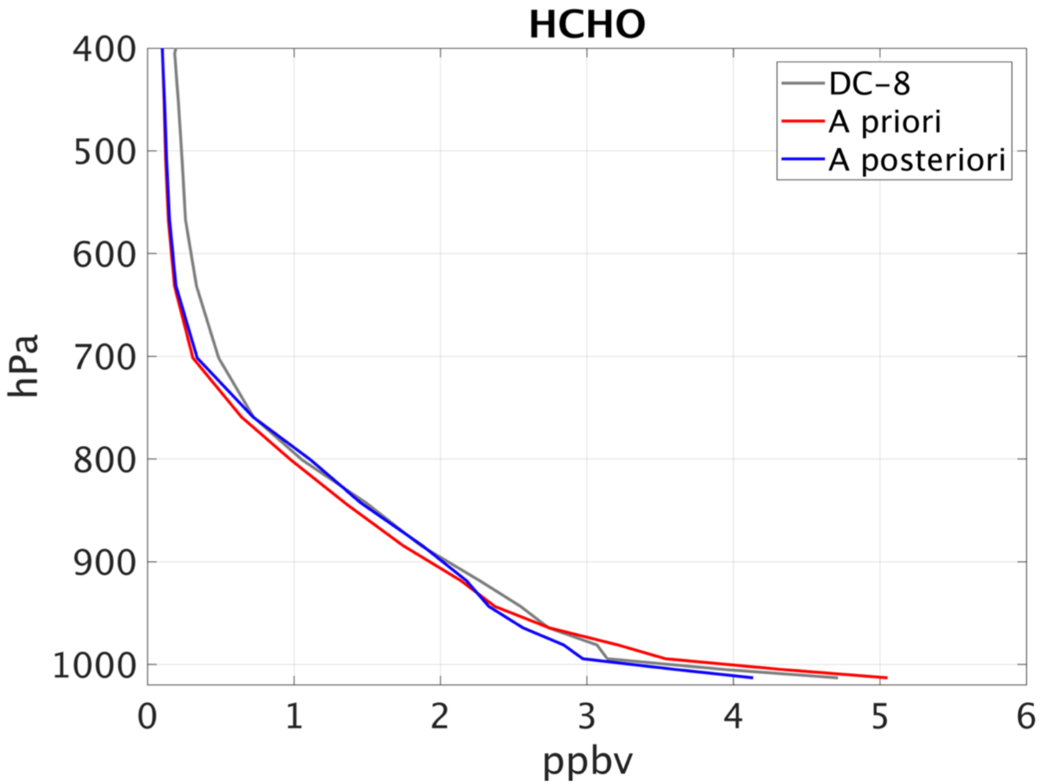

Figure S10. Comparison of the simulated model using the prior/posterior emissions and DC-8 measurements in terms of HCHO. We included all 10-secs observations available from DC-8 in May-June 2016. The profiles are the mean average.

OH and HO2 changes

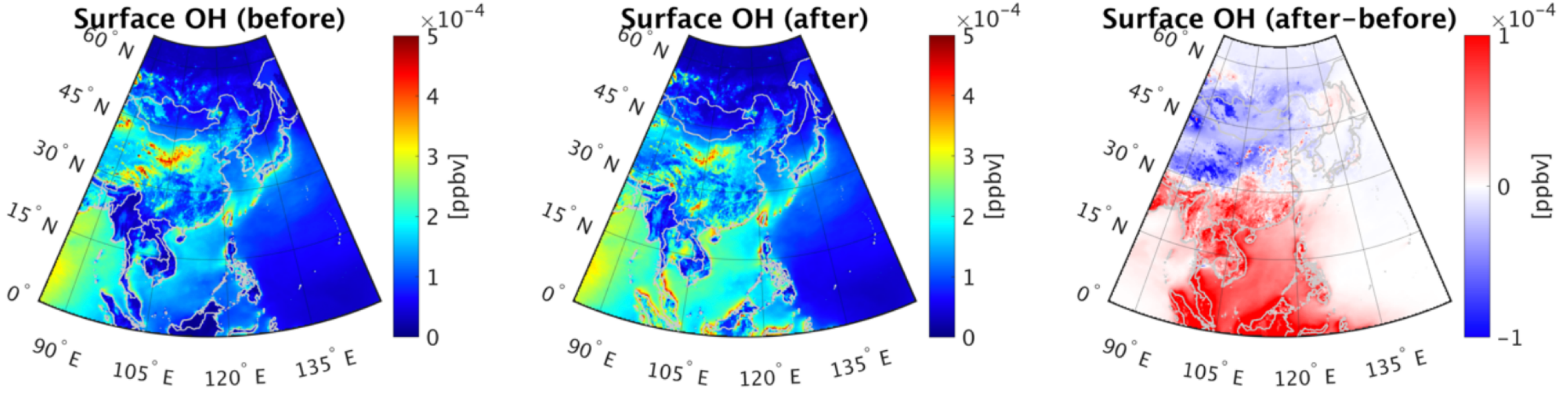

Figure S11. The simulations of surface OH before and after the inversion at 1200-1600 CST.

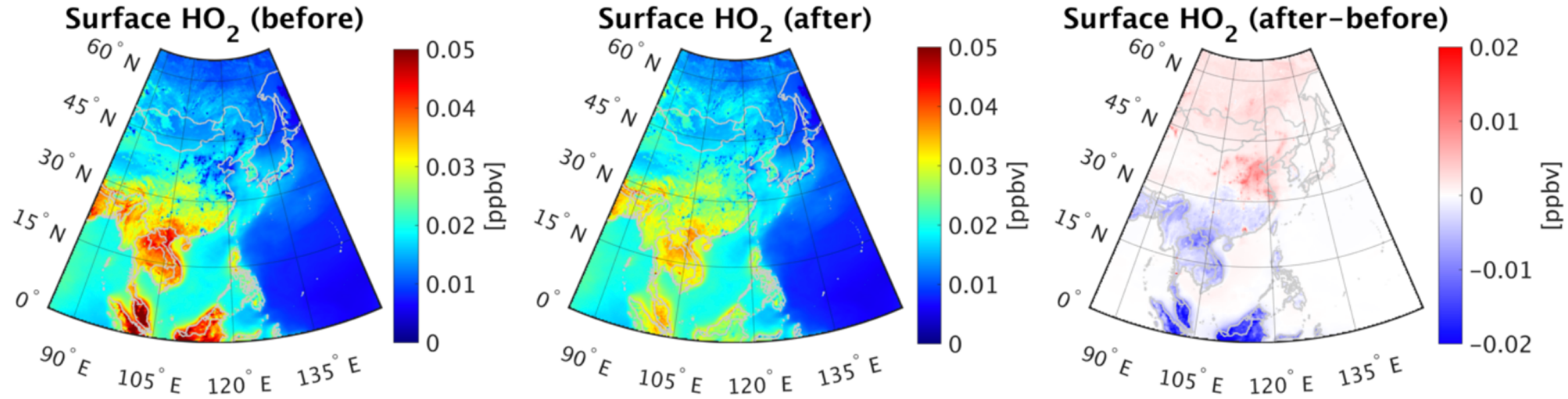

Figure S12. The simulations of surface HO_2 before and after the inversion at 1200-1600 CST.